An *LCC-C* Compensated Wireless Charging System for Implantable Cardiac Pacemakers: Theory, Experiment, and Safety Evaluation

Chunyan Xiao, *Member, IEEE*, Dingning Cheng, and Kangzheng Wei

***Abstract*—The technique of wireless power transfer (WPT) via magnetic coupling resonance provides a way to transfer power wirelessly to cardiac pacemakers from external source. For wireless charging system to be used in clinical environment, this paper gives priority consideration to three technical difficulties, i.e., implantation, efficiency, and safety. The *LCC-C* compensation topology for pacemaker wireless charger is presented, where only one secondary side resonance capacitor needs to be implanted, and resonance compensation parameters are derived. The compensation network can make the WPT system operate at stable resonance and high efficiency. The prototype of the wireless charging system for implantable cardiac pacemaker is developed, where a thin flexible receiving unit was designed to effectively shield eddy currents in the pacemaker shell. The experiments of wireless charging through pork tissues reveal that 3.072-W power can be received from a 3.919-W power source at 300 kHz, reaching a rather high WPT efficiency of 78.4%, such that the charging is fast, i.e., the 1050 mA·h, 4.2-V Li-ion battery voltage increases from 3.98 (80% residual capacity) to 4.2 V within only 27 min, and only 3.3 °C maximum temperature rise of the pork is in safe limits. The feasibility and safety of the charging system were further evaluated by simulations of specific absorption rate and temperature rise in human tissues and electromagnetic fields in the pacemaker case.**

***Index Terms*—Electromagnetic compatibility (EMC), implantable cardiac pacemaker, *LCC-C* compensation networks, magnetic coupling resonance (MCR), specific absorption rate (SAR), temperature rise, wireless charging system, wireless power transfer (WPT).**

I. Introduction

IMPLANTABLE cardiac pacemakers have played an increasingly important role in treating a broad range of cardiac disorders, and have been widely recognized as lifesavers for the patients with cardiovascular diseases. However, as disposable batteries are used, the implantable pacemakers are suffering from a limited lifespan of 5–15 years, depending on such factors as the type of system being used and how often the system is used [1]–[3]. When the pacemaker battery is running low, the entire pacemaker unit must be replaced. The replacement can cause risks similar to those of the original surgery, including but not limited to rejection, infection, bruising at the pacemaker site, and adverse reactions to anesthetics.

A possible solution to this problem is replacing disposable batteries with rechargeable batteries. Recent years have witnessed the dramatic emergence of rechargeable batteries in medical technologies, such as dealing with congestive heart failure, atrial tachycardia, deep brain stimulation, cochlear implants, and developing monitoring-only systems [4]–[6]. Since rechargeable batteries can supply power for high consumption of energy and current, they can outperform the disposable batteries when applied to the implantable pacemakers. In addition to delivering shocks to hearts as disposable batteries do, rechargeable batteries can also supply energy enough to regulate pacemakers, log data of heart rhythms, and perform other functions such as wireless telemetry, multipointing pacemakers, etc. [7]–[9]. However, so far the pacemakers with rechargeable batteries have not been applied in clinical environment.

Using rechargeable batteries would require a wireless charging system. To achieve power supply for the pacemakers outside the human body, a transcutaneous wireless power transfer (WPT) technique should be developed. For applications of biomedical systems, various means of energy transfer have been studied, such as optics, ultrasound, and biological sources [10]–[12]. Wherein, the most established technique is wireless powering through electromagnetic induction. The original WPT systems based on the electromagnetic induction principle are similar to the transformer with double E-type of ferrite cores, and the primary side and secondary side are split apart to a certain air gap operating at a nonresonant state. These systems have been implanted to artificial hearts, artificial cochlear, capsule endoscopies, etc. [13]–[15]. To our best knowledge, [16] is the only study of the WPT for the cardiac pacemakers using the ferrite-core transformer and the wireless charging prototype by experiments is also realized in it. However, this kind of WPT is featured by short distance, and this system has such a large volume and a heavy weight that it is not conducive to implantation in the human body because of chunks of ferromagnetic materials used in the magnetic circuit.

A new WPT technique is the magnetic coupling resonance (MCR) WPT. It is also based on the electromagnetic induction

Manuscript received April 13, 2017; revised May 4, 2017 and June 25, 2017; accepted July 27, 2017. Date of publication August 3, 2017; date of current version February 22, 2018. This work was supported by the National Natural Science Foundation of China under Grant 51277006. Recommended for publication by Associate Editor J. Acero. *(Corresponding author: Chunyan Xiao.)*

The authors are with the School of Automation Science and Electrical Engineering, Beihang University, Beijing 100191, China (e-mail: xiao_chunyan@buaa.edu.cn; chengdingning@buaa.edu.cn; weikangzheng@buaa.edu.cn).

Color versions of one or more of the figures in this paper are available online at http://ieeexplore.ieee.org.

Digital Object Identifier 10.1109/TPEL.2017.2735441

principle, but it enables the system to transfer power at high efficiency or power at a midrange distance [17]–[22]. For a two-coupling-coil system, when the angular frequency of the power source equals the coupling resonant frequency of the transmitter circuit and of the receiver circuit, the system is in the resonant state. At this time, most electromagnetic energy can be transferred between two coils, so that the transfer efficiency is greatly improved. This system can save chunks of ferrite materials, even if only air-core coils are used, and can also transfer power at high efficiency. Therefore, it can significantly reduce the volume and the weight of implanted systems while keeping stable resonance. Campi *et al.* [23] studied the electromagnetic fields (EMFs) and the temperature produced by the pacemaker's MCR-WPT system in order to investigate feasibility and safety of the WPT system for pacemakers. However, the system used a resistance as the load and did not really achieve charging. Therefore, the current used in simulations was different from that in the actual charging system. The human body model in simulations was simplified as a cylinder that was not accurate. Xiao *et al.* [24] studied the effect of eddy current in the pacemaker shell, and investigated the precise implant position of receiving coils without ferrite shielding. In addition to mention, although the rechargeable battery and the wireless charging system with two coupling coils are acceptable in size and weight, researchers have tried to further decrease the volume of the implanted system. Research [25]–[27] proposed to remove the battery and supply power for electrodes directly by the receiving coil. However, if this technique was used as the wireless power supply, patients would find it inconvenient to wear and their safety could be threatened because the external magnetic fields must continuously supply power for the receiving coil. Therefore, the paper studied the MCR-WPT technique to realize the pacemaker charging for rechargeable batteries.

Three aspects of implantation, efficiency, and safety must be given priority consideration if the wireless charging system can be used in actual clinical environment. In order to improve the WPT efficiency, different compensation topologies have been proposed and implemented to tune the two coils operating under a resonant status. Four basic topologies are series–series, series–parallel, parallel–series, and parallel–parallel topology [28]. If the compensation capacitor is connected to the transmitting coil in parallel, the output voltage of the power source will directly add to the capacitor when the WPT system is powered on. If the compensation capacitor is connected to the transmitting coil in series, a large current of power source is necessary when the system is in the stable resonance or in the self-resonance because the transmitter impedance is low. To avoid problems existing in the series or parallel compensation and to achieve high efficiency for the WPT system, superior topologies have been proposed [29]–[33], such as an *LCL* compensation network between the converter and the transmitting coil [29], and a bidirectional *LC* compensation network at both primary and secondary sides [30]. In [31], a double *LCC* compensation network was established by connecting a capacitor in series with the transmitting coil instead of the inductor, which can reduce size and cost of the inductor. This network showed high WPT efficiency in the charging experiment for electric vehicles. To analyze the circuit model of the double *LCC* compensation network, the resistances of both sides are ignored, which causes few errors and it is effective for the two coupling coils made of litz wires. However, due to the limited implantation space for the pacemaker receiver unit, litz wires as the receiving coil are not better than the flexible thin printed circuit in terms of the volume and the integration with the pacemaker. Therefore, the double *LCC* compensation network and the circuit model are not suitable for the pacemaker WPT system. Compared with the reactance, the resistance of the receiving coil cannot be ignored. More importantly, implantation requires a small number of electronic components and small volume of the actual system. The current flowing through the receiving coil embedded in the human body should also be low; otherwise, tissues could get overheated. Therefore, one of the intentions of this paper is to present a compensation network suitable for the cardiac pacemaker.

This study intends to design and realize an effective and safe wireless charging system for pacemakers with rechargeable batteries, based upon the MCR-WPT technology. We focused on solving following three technical difficulties.

1) the resonance compensation network needs to have the characteristics of high efficiency, stable resonance, and being implantable;
2) two coupled coils should be designed to decrease the effect of eddy current in the pacemaker shell and to be as small as possible to be implanted;
3) the developed charging system should be safe, and the implanted parts should be small in size.

First, we present and build the *LCC-C* compensation circuit model of the pacemaker WPT system with two coupling coils and deduce the MCR impedance matching parameters for the network. The *LCC-C* compensation circuit refers to one inductance and two capacitors connected to the primary coil, and one capacitor connected to the secondary coil. Second, two coupling coils for pacemaker charging are designed, considering the implantation of the receiver unit and effects of eddy currents in the pacemaker shell on the induced voltage across the receiving coil. Next, the MCR-WPT charging prototype for the pacemaker is developed, and charging experiments and temperature tests are conducted on pork tissues. Finally, according to the related guidelines and standards of the electromagnetic radiation (mainly specific absorption rate (SAR) in the human tissues), and considering the human body's temperature limit and the electromagnetic compatibility (EMC) with pacemakers, the safety of the pacemaker charging system is further assessed by finite element method (FEM) simulations of the EMFs and thermal fields based on a high-resolution human anatomical model and the measured currents through the two coils. Results of experiments and simulations show that the wireless charging system for pacemakers designed and realized in this study is suitable for being effective in wireless power supply, safe and implantable for human bodies. This system is also cost efficient because it requires only a simple modification in the existing pacemakers. Therefore, our research can make a significant contribution to the development and application of the pacemaker wireless charging device.

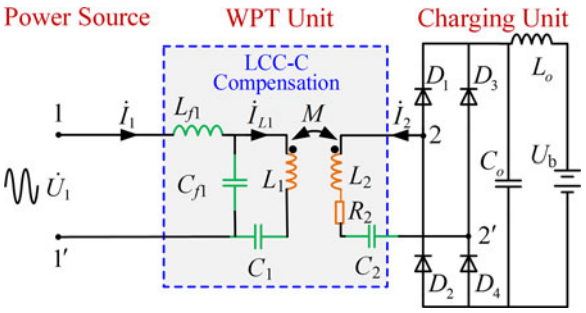

Fig. 1. Circuit model of wireless charging system with *LCC-C* compensation networks for implantable cardiac pacemakers.

II. *LCC-C* Compensation Circuit Topology Based on MCR

A. *LCC-C Compensation Network for MCR-WPT System*

Fig. 1 shows the circuit model of wireless charging system with *LCC-C* compensation networks for implantable cardiac pacemakers, which considers the resistance of the receiving coil. In the figure, the receiver unit uses only a capacitor in series to compensate the inductance of the receiving coil; thus, an inductance and a capacitor in *LCC* compensation circuit can be saved and the current through the receiving coil is relatively small. *LCC-C* compensation network is suitable for implantation because of its small number of implanted secondary compensation capacitor and due to the low current flowing through the implanted coil.

In Fig. 1, the inductances of the transmitting and receiving coil are L_1 and L_2, respectively. The resistance of the transmitting coil is ignored and the resistance of the receiving coil is R_2. The compensation capacitances on the transmitter side are C_1 and C_{f1}, whereas the compensation inductance is L_{f1}. Due to the small coupling coefficients between the compensation inductance L_{f1} and the inductances of two coils, we ignore their mutual inductances. The mutual inductance between the two coupling coils is *M*. In the following part, we deduce the impedance matching parameters of the *LCC-C* compensation network for MCR-WPT system and the WPT efficiency.

B. *Impedance Matching for Two-Port Network*

Due to coupling, the exchange of energy between the source and the receiver can be described by the two-port network. Suppose that the voltage between the port $1-1'$ is $\dot{U}_1$ (terminal 1 is +, terminal 1′ is –) and the voltage between the port $2-2'$ is $\dot{U}_2$ (terminal 2 is +, terminal 2′ is –). The currents flowing through the transmitting coil, the receiving coil, and the power source are $\dot{I}_{L1}$, $\dot{I}_2$, and $\dot{I}_1$, respectively. Their current reference directions are shown in Fig. 1. When the angular frequency is ω, the KVL equation of equivalent circuits in the frequency domain satisfies the following equations:

$$\begin{bmatrix}\dot{U}_1\\ \dot{U}_2\end{bmatrix}=\begin{bmatrix}Z_{11} & Z_{12}\\ Z_{21} & Z_{22}\end{bmatrix}\begin{bmatrix}\dot{I}_1\\ \dot{I}_2\end{bmatrix} \tag{1}$$

where

$$\begin{cases} Z_{11}=j\left[H_{11}-1/\left(\omega^2C_{f1}^2H_{12}\right)\right]\\ Z_{22}=R_2+j\left(H_{21}-\omega^2M^2/H_{12}\right)\\ Z_{12}=Z_{21}=-j\omega M/\left(\omega C_{f1}H_{12}\right)\end{cases} \tag{2}$$

$$\begin{cases} H_{11}=\omega L_{f1}-\left(\omega C_{f1}\right)^{-1}\\ H_{12}=\omega L_1-\left(\omega C_1\right)^{-1}-\left(\omega C_{f1}\right)^{-1}\\ H_{21}=\omega L_2-\left(\omega C_2\right)^{-1}\end{cases}. \tag{3}$$

We use the open-circuit short-circuit method to derive the network parameters. First, the voltage source $\dot{U}_1$ is applied on port $1-1'$. After solving the open-circuit voltage (OCV) and the short-circuit current (SCC) on port $2-2'$, the input equivalent impedance Z_{eq2} can be deduced. Then, port $2-2'$ is equal to an OCV source and an impedance Z_{eq2} in series according to Thevenin's theorem. Likewise, the voltage source $\dot{U}_2$ is applied on port $2-2'$ because the induced voltage across the receiving coil is equivalent to a voltage source. After solving the OCV and the SCC on port $1-1'$, the output equivalent impedance Z_{eq1} can be deduced. Then, port $1-1'$ is equal to an OCV source and an impedance Z_{eq1} in series. If the two-port networks in the WPT system operate in the resonant state, both the input impedance and the output impedance must reach the minimum values. Thus, the maximum transfer efficiency of WPT system can be achieved.

1) Input Equivalent Impedance Z_{eq2}: When the port $2-2'$ is open, we can obtain that the OCV $\dot{U}_{2\mathrm{OC}}=\dot{U}_2|_{\dot{I}_2=0}=\frac{Z_{12}}{Z_{11}}\dot{U}_1$; when the port $2-2'$ is short, we gain that the SCC $\dot{I}_{2\mathrm{SC}}=\dot{I}_2|_{\dot{U}_2=0}=\frac{Z_{12}}{Z_{12}^2-Z_{11}Z_{22}}\dot{U}_1$. Then, the equivalent impedance can be obtained as

$$Z_{\mathrm{eq2}}=\frac{\dot{U}_{2\mathrm{OC}}}{\dot{I}_{2\mathrm{SC}}}=\frac{Z_{12}^2-Z_{11}Z_{22}}{Z_{11}}. \tag{4}$$

Substituting (2) into (4) yields the equivalent impedance

$$Z_{\mathrm{eq2}}=R_2+j\frac{H_{21}+H_{11}\left(\omega^2M^2-H_{12}H_{21}\right)\omega^2C_{f1}^2}{1-\omega^2C_{f1}^2H_{11}H_{12}}. \tag{5}$$

2) Output Equivalent Impedance Z_{eq1}: When the port $1-1'$ is open, we can obtain that the OCV $\dot{U}_{1\mathrm{OC}}=\dot{U}_1|_{\dot{I}_1=0}=-\frac{Z_{12}}{Z_{22}}\dot{U}_2$; when the port $1-1'$ is short, we can gain that the SCC $\dot{I}_{1\mathrm{SC}}=\dot{I}_1|_{\dot{U}_1=0}=\frac{Z_{12}}{Z_{12}^2-Z_{11}Z_{22}}\dot{U}_2$. Then, the equivalent impedance can be written as

$$Z_{\mathrm{eq1}}=\frac{\dot{U}_{1\mathrm{OC}}}{\dot{I}_{1\mathrm{SC}}}=\frac{Z_{11}Z_{22}-Z_{12}^2}{Z_{22}}. \tag{6}$$

Substituting (2) into (6) yields the equivalent impedance

$$Z_{\mathrm{eq1}}=\frac{R_2\left(1-H_{11}H_{12}\omega^2C_{f1}^2\right)+j\left[H_{11}\left(\omega^2M^2-H_{12}H_{21}\right)\omega^2C_{f1}^2+H_{21}\right]}{\left[jR_2H_{12}+\left(\omega^2M^2-H_{12}H_{21}\right)\right]\omega^2C_{f1}^2}. \tag{7}$$

3) Resonance Impedance Matching Conditions: If the system is in the resonant state, the imaginary parts of the impedances on both sides should be zero, i.e., $\mathrm{Im}(Z_{\mathrm{eq1}})=0$ and $\mathrm{Im}(Z_{\mathrm{eq2}})=0$. From (5), we can obtain that one set of

solutions of $\mathrm{Im}(Z_{\mathrm{eq2}}) = 0$ is

$$H_{11} = 0 \,\text{and}\, H_{21} = 0. \tag{8}$$

Substitute (8) into (7), and then the impedance expression (7) when satisfying the matching condition of (8) becomes

$$Z_{\mathrm{eq1}} = \frac{R_2/\omega^2 C_{f1}^2}{\omega^2 M^2 + jH_{12}R_2}. \tag{9}$$

If (9) satisfies $\mathrm{Im}(Z_{\mathrm{eq1}}) = 0$, it requires that

$$H_{12} = 0. \tag{10}$$

From the above-mentioned derivations, simultaneously satisfying (8) and (10) can make the system resonant. We combine (8) with (10), and obtain the following set of solution:

$$\begin{cases} \omega^2 C_{f1} L_{f1} = 1 \\ \omega^2 C_1 \left(L_1 - L_{f1}\right) = 1 \\ \omega^2 L_2 C_2 = 1 \end{cases}. \tag{11}$$

It can be seen from (11) that by using this impedance matching method, the system is easy to achieve stable resonance. The main reasons are as follows: 1) The matching impedances of transmitter and receiver are decoupled. That is, the matching impedance at the transmitting end is only related to the circuit parameters at its own side, so is the receiving end. 2) The matching impedances of both ends are unrelated to the mutual inductance, i.e., when the two coils are misaligned or deflected, the system can still maintain stable resonance.

C. Currents Flowing Through the Two Coils

The magnitude and frequency of the currents flowing through the two coils will directly affect the electromagnetic radiation and the temperature rise in human tissues. Using voltages much higher than the minimum charging voltage will result in a higher current flow and faster charging, but it will cause a high power loss and swift intensification in temperature. Therefore, we must ensure a small current whose radiation and temperature rise pose no danger to the human body, while ensuring the battery can be charged to full as soon as possible.

When the *LCC-C* topology circuit is used, the current expressions of the transmitting coil and the receiving coil are

$$\dot{I}_{L1} = -j\frac{1}{\omega L_{f1}}\dot{U}_1 \tag{12}$$

$$\dot{I}_{L2} = \dot{I}_2 = \frac{1}{R_2}\left(\frac{M}{L_{f1}}\dot{U}_1 - \dot{U}_2\right). \tag{13}$$

From the expressions of (12) and (13), we can see that the currents flowing through the two coils proportionally increase as the voltage of power source increases. When the system is set up and supplied by a constant voltage source, a constant current flows through the transmitting coil and a constant voltage is induced across the receiving coil. Therefore, the transmitting coil has the characteristic of constant current source, which is different from the conventional series–series compensation network, $\dot{I}_{L1} = \frac{R_r + R_L}{(\omega M)^2}\dot{U}_1$; and the receiving coil has the characteristic of constant voltage source. Also, according to (12) and (13), the currents in two coils and the required power supply voltage $\dot{U}_1$ can also be reversely derived under the condition of meeting the charging voltage $\dot{U}_2$. If the load on the port $2-2'$ is R_L, that is $\dot{U}_2 = \dot{I}_{L2}R_L$, then (13) becomes

$$\dot{U}_1 = \frac{L_{f1}}{M}\left(R_2 + R_L\right)\dot{I}_{L2}. \tag{14}$$

From (14), the current $\dot{I}_{L2}$ is inversely proportional to the sum of the receiving coil's resistance and the load R_L, increases as the mutual inductance (the distance between two coils) increases, and decreases as the compensating inductance increases. If $L_{f1} = M$, then $\dot{U}_1 = \dot{I}_{L2}(R_2 + R_L)$. That is, the induced voltage across the receiving coil equals to the power supply's voltage, equivalent to the power supply connected directly to the receiver end.

D. Resonance Power Transfer Efficiency

When the WPT system is matched according to (11), the two-port network is in the resonant state. Then, the input power of port $1-1'$ or the output power of power source is as follows:

$$P_{\mathrm{in}} = \frac{M}{L_{f1}R_2}\left(\frac{M}{L_{f1}}\dot{U}_1 - \dot{U}_2\right)\dot{U}_1. \tag{15}$$

If the load is purely resistive, then the output power of port $2-2'$ or the input power of the load is as follows:

$$P_{\mathrm{out}} = \frac{1}{R_2}\left(\frac{M}{L_{f1}}\dot{U}_1 - \dot{U}_2\right)\dot{U}_2. \tag{16}$$

Then, the WPT efficiency of the two-port networks becomes

$$\eta = \frac{P_{\mathrm{out}}}{P_{\mathrm{in}}} = \frac{L_{f1}}{M}\cdot\frac{\dot{U}_2}{\dot{U}_1}. \tag{17}$$

From (17), the WPT efficiency of the two-port networks with *LCC-C* compensation is related with compensation inductance, the mutual inductance, and the voltages of two ports.

If the load is resistance R_L, then (17) becomes

$$\eta = \frac{1}{1 + R_2/R_L}. \tag{18}$$

From (18), to achieve a high efficiency for a WPT system, the resistance of the receiving coil should be decreased to a minimum possible value.

III. Wireless Charging System for the Implantable Cardiac Pacemaker

A. Prototype of the Wireless Charging System for the Implantable Cardiac Pacemaker

Referring to the dual- chamber cardiac pacemaker G70 produced by Medtronic Inc., with the size of 44.7 mm × 47.9 mm × 7.5 mm [34], we use the titanium alloy material TC4 with the thickness of 0.8 mm to make a metallic case of 31.4 mm × 47.4 mm × 8.1 mm, which fabricates the shell of the implantable cardiac pacemaker.

The wireless charging prototype for the implantable cardiac pacemaker, as shown in Fig. 2, mainly includes three parts: the power source, the WPT unit (consists of two coupling coils and *LCC-C* compensation network), and the charging unit. We

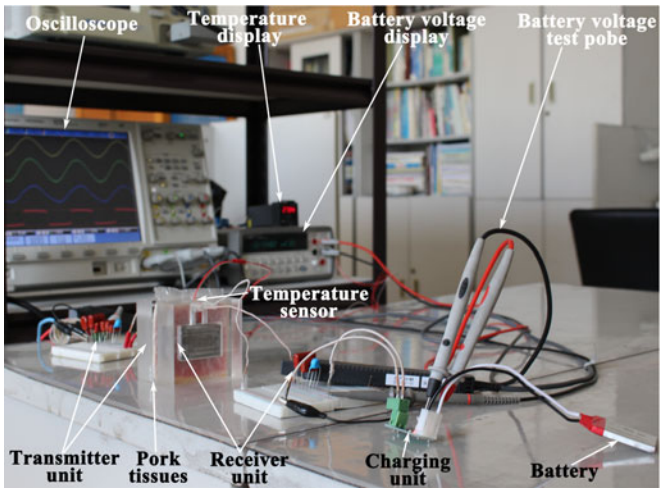

Fig. 2. Wireless charging prototype for the implantable cardiac pacemaker.

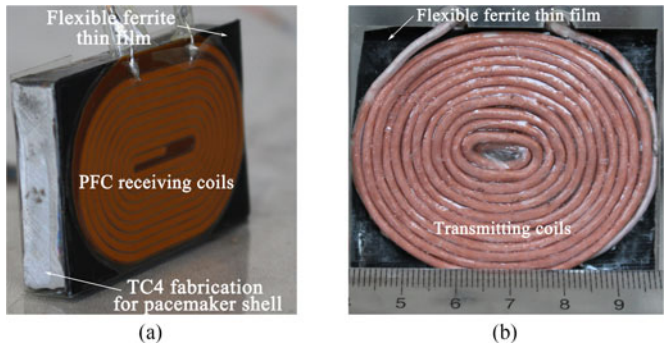

Fig. 3. Construction of two coupling coils in the wireless charging system for the implantable cardiac pacemaker. (a) Pacemaker shell fabrication and FPC receiving coil with thin ferrite film. (b) Transmitting coil with thin ferrite film.

TABLE I
PARAMETERS OF TWO COUPLING COILS

		Transmitter unit	Receiver unit
Two coupling coils	Layers	2	2
	Number of turns	13	9
	External dimensions/mm × mm	58 × 48	44.5 × 30.5
	Section dimensions/mm	Φ0.1 × 160	1.2 × 0.072
	Self-inductance/μH	16.21	11.73
	AC resistance/Ω	0.039	0.351
Ferrite film	Dimensions/mm × mm × mm	58 × 48 × 0.29	44.5 × 30.5 × 0.29

use signal generator DG1022U and dc power source BP4610 to generate 300-kHz sinusoidal ac power. Under the impedance matching of *LCC-C*, the transmitting coil emits the electromagnetic energy to the receiving coil at a distance of 8 mm. This 8-mm space is filled with 1-mm pigskin + 2-mm pig fat + 5-mm pork lean to simulate the skin and subcutaneous tissues of human body between the two coupling coils. Via the charging unit, the induced voltage signal received by the receiving coil is rectified and filtered. Then, the Li-ion battery SONY 633346 is charged at 450-mA constant current. The rated voltage of rechargeable battery is 4.2 V and its capacity is 1050 mA·h. In order to test the feasibility of MCR-WPT technology to generate voltages sufficient to charge the battery, a high-precision multimeter is attached to the battery for signal recording.

B. Two Coupling Coils for Implantable Cardiac Pacemakers

The eddy current produced in the metallic shell of the pacemaker seriously impacts the induced voltage across the receiving coil. Considering the efficiency and suitability of the WPT system for cardiac pacemaker, the two coils are designed to decrease the eddy current, to increase the coupling to achieve the WPT at a high efficiency, and to reduce the volume of the electronic system. The two coupling coils in the wireless charging system for the implantable cardiac pacemaker are shown in Fig. 3. Their dimensions are referred to the size of cardiac pacemaker G70 and parameters are shown in Table I.

The receiver unit consists of the receiving coil and a thin flexible ferrite film. The whole thickness is only 0.44 mm. It is fixed on the shell of the cardiac pacemaker fabrication as shown in Fig. 3(a). The receiving coil is designed as double layers, nine turns per layer, and it uses flexible printed circuit (FPC) with the shape of implantable cardiac pacemaker 44.5 mm × 30.5 mm, so it is thin and flexible. The 0.29-mm thickness of flexible ferrite film between the coil and the pacemaker shell is to provide the electromagnetic shielding to decrease the effect of eddy currents in the pacemaker shell. At the same time, the ferrite film can also increase the inductance and the mutual coefficients. The self-inductance of receiving coil is 11.73 μH and its ac resistance is 0.351 Ω. In actual applications, biomaterials with poor conductor need to be placed between the receiving coil and tissues to avoid the initiation of unwanted biological responses resulting from their direct contact. This is considered in the simulations, as shown in Section V.

The transmitter unit consists of the transmitting coil and a thin flexible ferrite film, as shown in Fig. 3(b). The transmitting coil employs the double-layer helical structure with 13 turns per layer, and connected with a flexible ferrite film. The transmitting coil uses litz wires, made of copper strand (160 leads with a diameter of 0.1 mm), to decrease the resistance. Considering the possible position offset between two coils, the external dimension of the transmitting coil is slightly larger than that of the receiving coil, with the oval shape of 58 mm × 48 mm. Thus, even if the offset happens, the receiving coil still can receive sufficient electromagnetic energy. The thin ferrite film also has the function of increasing the self-inductance and the mutual coefficient. The self-inductance of transmitting coil is 16.21 μH and its ac resistance is 0.039 Ω. This ac resistance is far less than its reactance (for example, the reactance is 30.555 Ω at the frequency of 300 kHz). Therefore, it is reasonable to build the circuit model that ignores the resistance of the transmitting coil while retaining the receiving coil's resistance, as shown in Fig. 1. The mutual inductance between two coils is $M = 4.88\ \mu$H, and the mutual coefficient is $k = 0.35$.

TABLE II
THEORETICAL AND MEASURED CIRCUIT PARAMETERS OF COMPENSATION COMPONENTS

Circuit parameters		Theoretical value	Measured value	ESR
Transmitter side	Inductance L_{f1}	—	2.82 μH	0.023 Ω
	Capacitance C_{f1}	99.80 nF	76.74 nF	0.13 Ω
	Capacitance C_1	23.99 nF	22.22 nF	0.69 Ω
Receiver side	Capacitance C_2	21.02 nF	25.24 nF	0.43 Ω

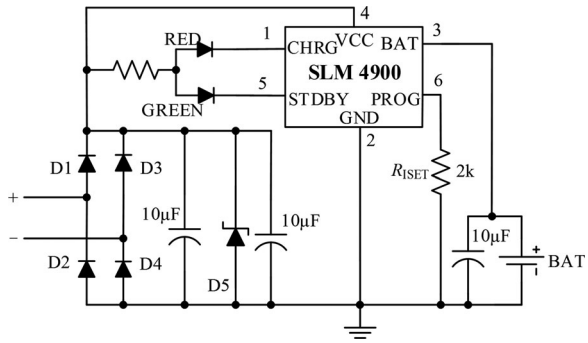

Fig. 4. Charging unit for rechargeable battery.

C. LCC-C Compensation Network for Resonance

Impedance matching for the *LCC-C* compensation network is one of the important steps to operate the system in the resonant state in order to achieve the maximum WPT efficiency in the charging experiments. The compensation inductance on the transmitter side L_{f1} is 2.82 μH and its resistance is 0.039 Ω. After the compensation is determined and based on (11), we can calculate a set of compensation capacitances at the resonant frequency of 300 kHz, $C_{f1} = 99.80$ nF, $C_1 = 23.99$ nF, and $C_2 = 21.02$ nF. Because of the equivalent series resistance (ESR) in the electronic components such as inductances and capacitance, there is a deviation between the actual value and the theoretical value. Their theoretical and measured parameters of compensation components are shown in Table II.

Under this matching, the measured voltage and current waveforms are shown in Fig. 5. From Fig. 5(a) and (b), we can see that the voltage and the current of both the power source and the load are in phase. At this time, the WPT system operates at the resonant state.

D. Battery Charging Unit

Considering the possible heating in human tissues caused by the heat loss as well as the psychological state of patients, the charging time should not be too long. In our study, the whole charging time of the designed charging system for cardiac pacemaker is within a short duration of 30 min. Miniaturization of the system is also crucial for the effectiveness of the system and for patients' safety. Therefore, the charging circuit designed here not only achieves the fundamental functions, but also takes a simple circuit topology and uses the electronic components with the smallest volume. This charging unit for the rechargeable

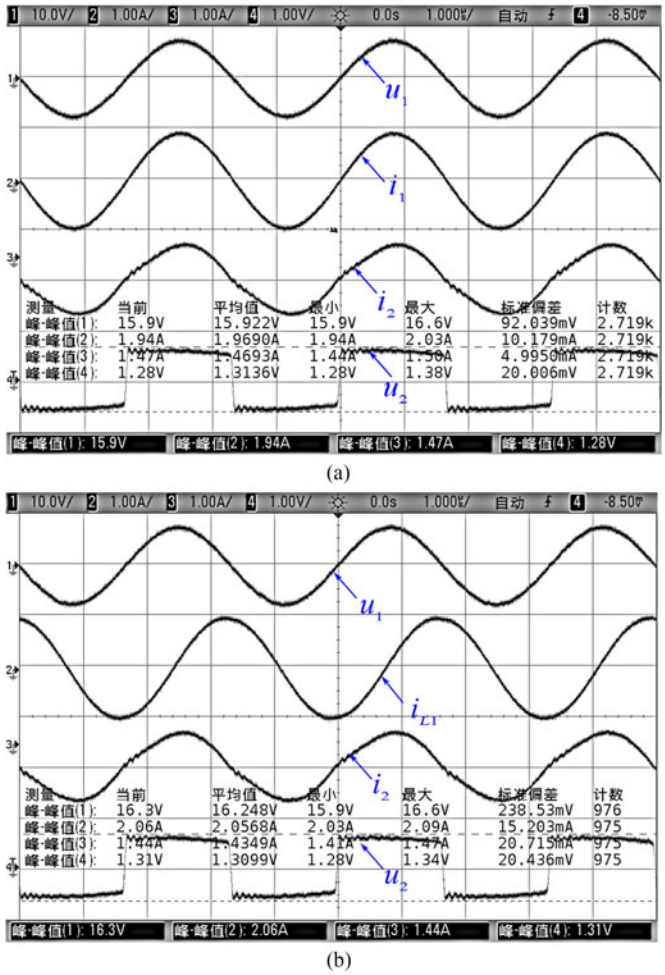

Fig. 5. Measured waveforms of voltages and currents. (a) Voltages and the currents of the power source and the load. (b) Current flowing through the transmitting coil.

battery includes a rectifier, a filter circuit, voltage-stabilizing circuits, a charging management IC, etc., as shown in Fig. 4. In the rectifier part, the forward voltage of rectifier diodes and the mode of rectification are two important factors that influence the WPT efficiency. The system uses a full-bridge rectifier, making the most use of the energy on the positive and negative cycles. The rectifier diode uses 1N5819, which is small in size, large in the forward current, and low in the voltage drop. In order to reduce the size of the structure, we use 5.1-V voltage-regulator diode directly, and then connect a capacitor in parallel to reduce the voltage ripple and to further regulate the voltage. The charging management IC SLM4900 charges in the mode of constant voltage and constant current, and the voltage range is from 4.5 to 6.5 V.

IV. EXPERIMENTS OF CHARGING AND TEMPERATURE MEASUREMENT

In the process of experiments, the parameters of the power supply and the matching network remain the same as the initial values. The battery voltage is charged from 3.98 to 4.20 V. The corresponding relationships between OCV and the residual

TABLE III
MEASURED CURRENTS AND VOLTAGES AND CALCULATED POWER DISTRIBUTIONS

Transmitter side	Peak–peak voltage on power source/V	15.922
	Peak–peak current through power source/A	1.9690
	Peak–peak current through transmitting coil/A	2.0568
Receiver side	Peak–peak voltage across load/V	13.136
	Peak–peak current through load/A	1.4693
Power distributions	Output power of power supply/W	3.919 (100%)
	Input power of the load/W	3.072 (78.4%)
	Receiving coil heat loss/W	0.095 (2.4%)
	Transmitting coil heat loss/W	0.021 (0.5%)
	Compensation inductance heat loss/W	0.011 (0.3%)
	Ferrite loss, electromagnetic leakage between two coupling coils, tissue heat loss, and stray losses/W	0.713 (18.4%)

capacity of standard 4.20-V Li-ion battery are as follows: When the battery's residual capacity reaches 100%, 90%, and 80%, the corresponding OCV is 4.20, 4.06, and 3.98 V, respectively.

In order to calculate the power and the efficiency of the WPT system, we apply Oscilloscope Agilent DSO 7034A to record the waveforms of voltages and currents of the power source and the load. In order to assess the safety and feasibility of the charging system by simulations of EMFs and thermal fields in Section V, we also measure and record the currents of the transmitting coil and the receiving coil. Every minute, the battery voltage and the temperature on the interface between the receiving coil and the pork lean meat are recorded.

A. WPT Power and Efficiency of the Charging System

The waveforms of voltages and currents are measured and shown in Fig. 5. Fig. 5 shows that both the voltage of port $1-1'$ and the current flowing through the power source are sinusoidal. Their peak-to-peak values $U_{\rm in}^{\rm p-p}$ and $I_{\rm in}^{\rm p-p}$ are 15.922 V and 1.9690 A, respectively, and their corresponding values of root mean square (rms) are 5.629 V and 0.6961 A, respectively. The current flowing through the transmitting coil is also the sinusoidal waveform and its rms value is 0.7272 A. The part connected to the port $2-2'$, as shown in Fig. 1, is taken as the load where the load voltage is approximately square wave with the peak-to-peak value $U_{\rm out}^{\rm p-p}$ of 13.136 V. Waveform for the current flowing through the load or the receiving coil is close to the sinusoidal wave. Its peak-to-peak value $I_{\rm out}^{\rm p-p}$ is 1.4693 A, and correspondingly, its rms value is 0.5195 A.

The values of the current, the voltage, and the calculated power distributions for each power consumption are shown in Table III. The following is the average input power of the two-port networks over one cycle *T*, i.e., the average output power of power source:

$$P_{\rm in}=\frac{1}{T}\int_0^T p_{\rm in}dt=\frac{4}{T}\int_0^{T/4}\left(\frac{1}{2}I_{\rm in}^{\rm p-p}\cos\omega t\cdot\frac{1}{2}U_{\rm in}^{\rm p-p}\cos\omega t\right)dt$$
$$=\frac{1}{8}U_{\rm in}^{\rm p-p}I_{\rm in}^{\rm p-p}. \tag{19}$$

The following is the average output power of the two-port networks over one cycle, or the load average input power:

$$P_{\rm out}=\frac{1}{T}\int_0^T p_{\rm out}dt=\frac{4}{T}\int_0^{T/4}\left(\frac{1}{2}I_{\rm out}^{\rm p-p}\cos\omega t\cdot\frac{1}{2}U_{\rm out}^{\rm p-p}\right)dt$$
$$=\frac{1}{2\pi}U_{\rm out}^{\rm p-p}I_{\rm out}^{\rm p-p}. \tag{20}$$

Then, we can obtain the WPT efficiency as

$$\eta=\frac{P_{\rm out}}{P_{\rm in}}=\frac{4}{\pi}\cdot\frac{U_{\rm out}^{\rm p-p}I_{\rm out}^{\rm p-p}}{U_{\rm in}^{\rm p-p}I_{\rm in}^{\rm p-p}}. \tag{21}$$

We substitute the values of the measured voltage and current in Table III to (21) and calculate the WPT efficiency $\eta=78.4\%$. The efficiency measurement only considers the power losses in the two-port network. After calculations, we obtain the heat losses on the receiving coil, the transmitting coil, and the compensation coil, which are 0.095, 0.021, and 0.011 W, respectively, totaling around 3.2%. The power loss of 18.4% is compounded by the ferrite loss, the loss of electromagnetic leakage between the two coupling coils, tissue heating, and ESR heating of the capacitance. Given the inevitable loss of power, the WPT efficiency of our charging system for cardiac pacemaker is relatively high when comparing with the currently reached efficiency [23], [35]. The main reasons are: 1) For the low power transfer system with watt level or below, comparing with its transfer power, the conductor loss and the stray loss of the components cannot be ignored at high frequency. It is noted that considering the safety of the human body and the WPT efficiency, the frequency cannot be too low. 2) Due to the limited implant space for the receiving coil, the flexible PCB coil is better than that made of litz wire. Therefore, it is difficult to further increase the mutual inductance and to decrease the resistance loss. If the system can transfer the power in a high efficiency, the power transferred through the human tissues will be decreased, leading to low electromagnetic radiation and temperature rise.

B. Battery Voltages Measured When Charging

Fig. 6 shows how the measured battery voltages vary with time in the experiment. As it can be seen, the whole charging process lasts only 27 min, less than half an hour, but the battery voltage rises from 3.98 to 4.2014 V. The Li-ion battery is charged from 80% of residual capacity to 100%, showing a substantial increase of 20%. With the increased capacity, the cardiac pacemaker can gain an extra lifespan of at least 2.4 years when the pacemaker operates at the current of 10 μA. These results show that the wireless charging system designed in this study works rather effectively in charging the batteries in the cardiac pacemaker. In addition, the charging time is short so that the

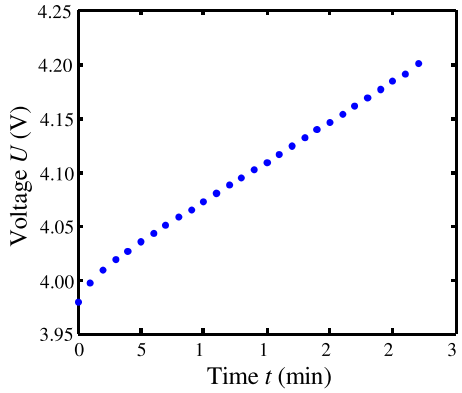

Fig. 6. Measured battery voltages vary with time.

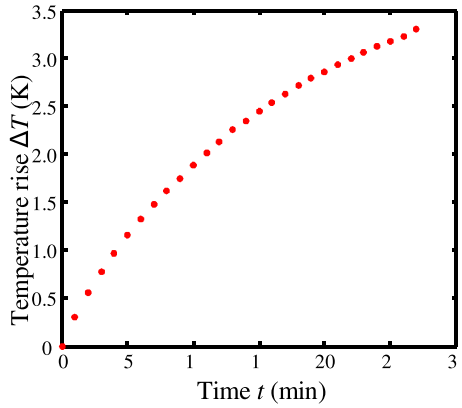

Fig. 7. Temperature rise at the interface between the receiving coil and tissues.

users of the pacemaker will not experience any psychological stress.

C. Temperature Measured When Charging

At the beginning of experiments, the apparatus is fully cooled to the room temperature of 25.67 °C. The temperature sensor is placed on the interface between the receiving coil and the tissues, which is the approximate location of the maximum temperature rise.

The temperature is recorded every minute and the changes are shown in Fig. 7. In spite of the rising tendency in the process of charging, the temperature increase remains less than 3.3 °C within 27 min. According to human physiology [36], large elevations of body temperature, which is beyond the precise regulatory mechanisms, will cause nerve malfunction and protein denaturation. Some people suffer convulsions at a body temperature of 41 °C, and 43 °C is considered to be the absolute limit for survival. Although this temperature restriction is for the whole body rather than the localized tissues, in this study we use 41 °C as the basic temperature restriction. Therefore, the maximum temperature rise of 3.3 °C in the local tissues causes no damage to the human body.

Given the different conditions between the experiment and the real human body, the heat radiations in the experiments are supposed to be faster than that in the human body. For one reason, experiments employ pork rather than *in vivo* tissues, which has a low heat dissipation because of the lack of convection caused by blood flow; for another, the environmental temperature is lower than the human body temperature. Therefore, safety issues of the implanted system must be further examined in the simulations because the electronic systems implanted in the human body must have lower clinical risks for patients.

TABLE IV
BASIC RESTRICTIONS (WBSAR, PSSAR$_{10\,g}$) FOR OCCUPATIONAL EXPOSURE SPECIFIED BY ICNIRP AND IEEE C95.1

	Frequency range	Whole-body average SAR (W/kg)	Localized SAR (head and trunk) (W/kg)	Localized SAR(limbs) (W/kg)
ICNIRP	100 kHz–10 MHz	0.4	10	20
IEEE	100 kHz–3 GHz	0.4	10	20

V. SAFETY EVALUATIONS OF THE WIRELESS CHARGING SYSTEM BY SIMULATIONS OF ELECTROMAGNETIC RADIATION AND THE TEMPERATURE RISE OF TISSUES

After achieving high efficiency of charging with the MCR-WPT, we evaluate the issue about the feasibility of using this technique. Several concerns include potential health effects due to EMF exposures, and the EMC between the wireless charging device and the cardiac pacemaker.

A. Guidelines and Standards

The basic restriction, as already demonstrated in [37], is a more appropriate metric for localized exposure evaluation than the reference level (i.e., the incident field intensity). The basic restrictions for SAR and the current density provided by the International Commission on Non-Ionizing Radiation Protection (ICNRP) [38] and the Institute of Electrical and Electronics Engineers (IEEE) [39] are used for the compliance assessment. Therefore, the occupational exposure basic restrictions suggested in ICNIRP and IEEE Std C95.1 are employed as the basis for exposure compliance assessment. It should be noted that ICNIRP, which also employs current density as the basic restriction quantity at low frequency, is referred only for the SAR limit in this study. For a localized exposure scenario, localized SAR averaging mass is any 10 g of contiguous tissue; the maximum $\mathrm{SAR}_{10\,\mathrm{g}}$ so obtained should be the value used for the estimation of exposure. In addition to the 10-g tissue average peak spatial SAR ($\mathrm{psSAR}_{10\mathrm{g}}$), the whole-body average SAR (wbSAR) is also specified as a relevant dosimetric quantity by ICNIRP and IEEE. The frequency range across which SAR is required to be assessed is from 100 kHz to 10 MHz for the ICNIRP guidelines and from 100 kHz to 3 GHz for the IEEE standards. The basic restrictions relevant to this paper are presented in Table IV.

In addition to SAR, which should be estimated for an implanted medical device, the temperature rise of tissues also needs to be investigated. Therefore, concerns of the system's

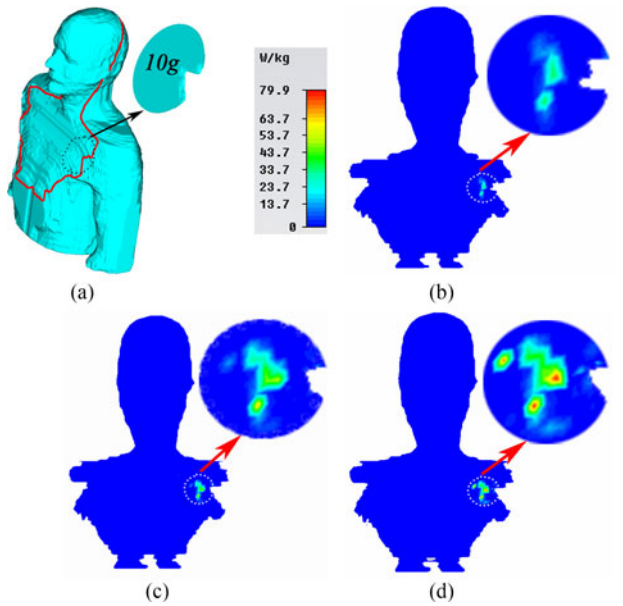

Fig. 8. Sliced figures of SAR in the human tissues produced by the WPT charging system for the implantable cardiac pacemaker. (a) Slice position and 10-g tissues, (b) 0.86 mm, (c) 0.36 mm, and (d) 0.06 mm over the interface between tissues and biomaterials.

TABLE V
CONDUCTIVITY AND RELATIVE PERMITTIVITY OF TISSUES AND PACEMAKER SHELL AT 300 KHZ

Parts	ε_r	$\sigma/S\,m^{-1}$
Head (including brain)	1569.4	0.1452
Heart	4577.0	0.2547
Lung	1327.1	0.1168
Chest	5226.9	0.4069
Subcutaneous fat	64.1	0.0436
Interior of pacemaker case	1	0
Pacemaker shell	5	2.38×10^6

safety include SAR and temperature rise in human tissues as well as EMC with the pacemaker. In the following, we first assess the safety in the human tissues by simulations of EMFs and thermal fields, based on the measured currents 0.7272 A through the transmitting coil and 0.5159 A through the receiving coil, respectively. Then, we examine the possibility of electromagnetic interference produced by the charging system with the internal electronic components and equipment in the artificial pacemaker case.

B. FEM Simulation Model of the EMFs and Thermal Fields

In order to accurately simulate the WPT performance, a high-resolution anatomical upper body model is built by using FEM software, as shown in Fig. 8(a). The model is composed of head, brain, heart, lung, skin, fat, muscle, etc. The complex permittivities (a function of frequency) of these human tissues at the frequency of 300 kHz are calculated and set based on Gabriel *et al.* [40], as shown in Table V.

At this frequency, the electromagnetic absorption by the human body causes heating effect rather than nonthermal effect and accumulative effect. Tissue absorption and heating are mainly from the radiative loss, ohmic wire loss, ohmic tissue loss, ferrite loss, etc. In the temperature simulations, we suppose the initial temperature of human body is 36.5 °C. Therefore, the limit of the temperature rise is 4.5 °C. As mentioned earlier, to avoid the receiving unit's direct contact with tissues, 2.2-mm thickness of biomaterials is placed between the tissues and the receiving unit with 0.44-mm thickness.

C. SAR and Temperature Rise in the Human Tissues and EMFs in the Pacemaker Case

1) SAR in the Human Tissues Produced by the Wireless Charging System: Table VI shows the SAR and the temperature rise in the human body produced by the WPT system. It can be seen from Table VI that for the head (containing the brain), the maximum SAR $\mathrm{SAR}_{\max}$ is only 5.12×10^{-6} W/kg. Therefore, the brain function will not be impaired. As for the heart, the value of $\mathrm{SAR}_{\max}$ is 4.74×10^{-6} W/kg, larger than those of head because of its closer distance to wireless charging system than the head, but it is still in the safety range. For the lungs, the value of $\mathrm{SAR}_{\max}$ is larger than those of either head or heart because the lungs are directly under the charging system. The $\mathrm{SAR}_{\max}$ is 4.04×10^{-5} W/kg, which is still safe. For the whole upper body, the $\mathrm{SAR}_{\max}$ of 79.7 W/kg appears in the chest muscle between the transmitting coil and the receiving coil, which is just under the transmitting coil and 2.7 mm over the lower surface of the receiving unit, that is in the tissues 0.06 mm over the interface between tissues and biomaterials, as shown in Fig. 9(b).

Fig. 8 shows the sliced figures of SAR in the human tissues produced by the WPT charging system for the implantable cardiac pacemaker. Slices are paralleled to the receiving coil and the transmitting coil, as shown in Fig. 8(a). Fig. 8(b)–(d) show the SARs in the human tissues of 0.86, 0.36, and 0.06 mm over the interface between tissues and biomaterials, respectively. Comparing these three figures, we can see that the closer the distance to receiving coil is, the greater the SAR value is. Fig. 8(b) shows the very small SAR value in the human tissues, whereas Fig. 8(d) shows that the maximum SAR of 79.9 W/kg occurs in the local human tissues.

After locating the $\mathrm{SAR}_{\max}$, we take 10-g human tissues containing the $\mathrm{SAR}_{\max}$ point, as shown in Fig. 8(a). This 10-g tissue average peak spatial SAR $\mathrm{psSAR}_{10\,\mathrm{g}}$ is 2.89 W/kg, which is less than the restriction of 10 W/kg recommended by ICNIRP and IEEE. Similarly, the whole upper body average SAR wbSAR is 0.012 W/kg, which is much less than the limit of 0.4 W/kg. Therefore, the human body SAR produced by the wireless charging system is safe and cannot cause the accumulative effect by heat.

2) Temperature Rise of Tissues: As above analysis of the power distributions in Table III, the heating in tissues and pacemakers is the result of resistive losses in the circuitry, eddy currents in the pacemaker case, contributions coming from the SAR, exothermic reaction in the components and batteries, etc. Note that despite the low electrical conductivity, the human tissues still cause eddy current losses because of their SARs, which

TABLE VI
SAR AND THE TEMPERATURE RISE IN THE HUMAN BODY PRODUCED BY THE WPT SYSTEM

Parts		Head (including brain)	Heart	Lung	Chest	Subcutaneous fat (chest)	The whole body (upper body)
SAR/W·kg^{-1}	$\mathrm{psSAR}_{10\tilde{}g}$	—	—	—	2.89	—	—
	wbSAR	—	—	—	—	—	0.012
	$\mathrm{SAR}_{\max}$	5.12×10^{-6}	4.74×10^{-6}	4.04×10^{-5}	79.9	57.1	79.9
	$\mathrm{SAR}_{\min}$	2.00×10^{-9}	2.71×10^{-8}	5.58×10^{-10}	1.05×10^{-6}	1.96×10^{-5}	0
ΔT/°C	$\Delta T_{\max}$	0.19	0.46	1.07	4.22	4.21	4.22
	$\Delta T_{\min}$	0.008	0.229	0.19	0.64	0.63	0

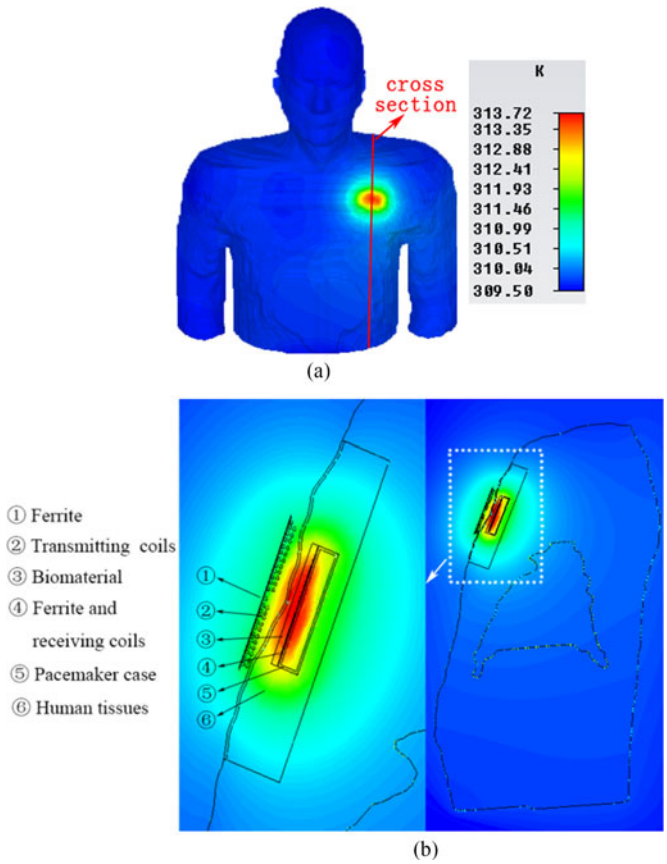

Fig. 9. Temperature distributions in the human body produced by the wireless charging system for cardiac pacemaker (a) in the upper body and (b) on the cross section.

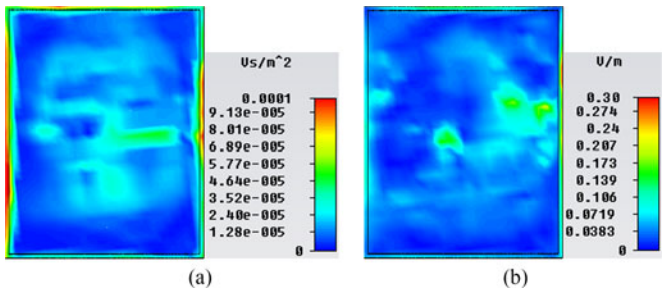

Fig. 10. EMFs on the cross section of 3 mm under the upper surface of the pacemaker case. (a) Magnetic flux density. (b) Electric field intensity.

in turn results in the temperature rise. From Table VI, we can also see that the maximum temperature rise $\Delta T_{\max}$ for the head (containing the brain), the heart, and the lungs are, respectively, 0.19, 0.46, and 1.07 °C, which are safe. For the whole body, the $\Delta T_{\max}$ of 4.22 °C appears at the same position with that of $\mathrm{SAR}_{\max}$, still in the safe range.

Fig. 9 shows the thermal distributions in the human body generated by the wireless charging system for artificial pacemaker. Fig. 9(a) shows the temperature distributions in the whole human body, and also shows the cross section of Fig. 9(b). It can be seen from Fig. 9(a), that the temperature rise in the human tissues mainly occurs in the region between the transmitting coil and the receiving coil. The closer the region is to the central axis of two coils, the greater the temperature rise is. Fig. 9(b) shows that the temperature rise is higher when the tissues are closer to the receiving coil, and the highest temperature rise is 4.22 °C, which cannot cause the heat damage. In the actual applications, we will use some cooling measures to cool down the human tissues.

3) EMFs Inside the Pacemaker Case: In order to assess whether the EMFs produced by the wireless charging system will affect the normal operation of the electronic components and systems in the pacemaker case, that is whether the charging system is electromagnetically compatible with the cardiac pacemaker, we calculate the electric and magnetic fields generated in the pacemaker case. Fig. 10 shows the magnitudes of electric field intensity E and the magnetic induction density B inside of the titanium alloy artificial pacemaker case, locating at 3 mm from the upper surface of the pacemaker case. It can be seen that the EMF in the pacemaker shell is much larger than that inside of the case. The maximum electric field intensity inside of the case is 0.217 V/m. For example, if the transmission line is 1 mm, the induced voltage across the line is less than 0.217 mV. The maximum magnetic induction density is 49.5 μT, which is almost the same as the magnitude of the Earth's magnetic field. These results show that the thin ferrite film of the receiver unit cannot completely shield the EMF. However, combining the ferrite film with the metal shell of the pacemaker, the EMFs in the pacemaker case decrease to a very small value. In short, the wireless charging system and the cardiac pacemaker are electromagnetically compatible.

VI. CONCLUSION

This study has successfully developed a prototype of wireless charging systems for the implantable cardiac pacemakers. Findings demonstrate that the transcutaneous MCR-WPT technique

is feasible for the cardiac pacemakers. The specific contributions and conclusions of this study are listed as follows.

1) A special topology of *LCC-C* compensation circuit is proposed, and its resonant impedance matching parameters are derived. The compensation network has been proved to be suitable for the wireless charging system for implantable cardiac pacemakers. There are three underlying principles of this proposal. First, the power is transferred to the receiving coil at high efficiency and stable resonance. The transmitting coil has the characteristic of constant current source, and the receiving coil have the characteristic of constant voltage source. Second, the number of secondary side resonance compensation capacitor implanted in the human body is as few as possible. Third, the current through the receiving coil is low enough to avoid overheating human tissues.
2) The new transmitting and receiving units for cardiac pacemaker wireless charging are designed. The receiver unit is thin and flexible. It adopts a thin flexible ferrite film to reduce the eddy current in the cardiac pacemaker case, thus the WPT efficiency is improved. It is also proved to be suitable to be implanted into the human body due to its small volume. A thin flexible receiving unit is integrated on the top surface of the pacemaker case, and only needs slight modifications to the existing pacemaker. The larger size of transmitting coil than that of receiving coil can ensure the power transferred stably.
3) The wireless charging prototype for the cardiac pacemaker is developed, which achieves high power transfer through 8-mm pork tissues at high efficiency. It can receive 3.072 W from a 3.919-W power source at the frequency of 300 kHz. The WPT efficiency is very high, reaching 78.4%. The 1050 mA·h, 4.2-V Li-ion battery can be charged to 4.2 V from the residential capacity of 80% in a short time span of 27 min. Meanwhile, in the absence of any additional cooling or heat measures, the maximum temperature rise of the local tissue is less than 3.3 °C, which will not harm the human body. Therefore, the experimental results show that the charging system is suitable for implantation, efficient and safe, and the short charging time will not cause the patients psychological stress.
4) The feasibility and safety of the charging system are also evaluated by simulations based on high-resolution anatomical models. Results reveal that the charging system is safe for the human tissues as well as electromagnetic compatible with the cardiac pacemaker. The details are: the 10-g tissue average peak spatial psSAR_{10g} is 2.89 W/kg, and the whole upper body average SAR is 0.012 W/kg; the maximum temperature rise that occurs in the point tissue is 4.22 °C; the maximum electric field intensity and magnetic induction density in the pacemaker case are 0.217 V/m and 49.5 μT, respectively.

In conclusion, the presented technique supports the successful development of cardiac pacemaker wireless charging system with characteristics of safety and effectiveness as well as short charging time. The developed wireless charging system can be applied to the existing pacemakers by only simple modifications to the present pacemakers. Further studies still need to perform tests on animals and finally conduct the clinical testing in order to facilitate the introduction of the wireless charging system to the actual applications. The results in this paper are useful for both practicing engineers and researchers who design and evaluate similar WPT systems.

REFERENCES

[1] M. Santini *et al.*, "Current state of knowledge and experts' perspective on the subcutaneous implantable cardioverter-defibrillator," *J. Interventional Cardiac Electrophysiol.*, vol. 25, no. 1, pp. 83–88, Jun. 2009.

[2] J. G. Webster, *Medical Instrumentation Application and Design*, 4th ed. Hoboken, NJ, USA: Wiley, 1999.

[3] J. Drews, G. Fehrmann, R. Staub, and R. Wolf, "Primary batteries for implantable pacemakers and defibrillators," *J. Power Sources*, vol. 97–98, no. 7, pp. 747–749, Jul. 2001.

[4] C. L. Schmidt and P. M. Skarstad, "The future of lithium and lithium-ion batteries in implantable medical systems," *J. Power Sources*, vol. 97–98, no. 3, pp. 742–746, Jul. 2001.

[5] K. Goto, T. Nakagawa, O. Nakamura, and S. Kawata, "An implantable power supply with an optical rechargeable lithium battery," *IEEE Trans. Biomed. Eng.*, vol. 48, no. 7, pp. 830–833, Jul. 2001.

[6] O. Jimenez, G. Echarri, J. E. Kast, J. E. Riekels, and M. E. Schommer, "Method of charging an implantable medical system," U.S. Patent 8 170 681 B2, May 1, 2012.

[7] S. Y. Lee *et al.*, "A programmable implantable microstimulator SoC with wireless telemetry: Application in closed-loop endocardial stimulation for cardiac pacemaker," *IEEE Trans. Biomed. Circuits Syst.*, vol. 5, no. 6, pp. 511–522, Dec. 2011.

[8] R. Das and H. Yoo, "Biotelemetry and wireless powering for leadless pacemaker systems," *IEEE Microw. Wireless Compon. Lett.*, vol. 25, no. 4, pp. 262–264, Apr. 2015.

[9] M. Limousin, "Methods and apparatus for controlling atrial stimulation in a double atrial triple chamber cardiac pacemaker," U.S. Patent 5 514 161 A, May 7, 1996.

[10] F. Robicsek and R. P. Morency, "Apparatus and method for activating a pump in response to optical signals from a pacemaker," U.S. Patent 4 827 906 A, May 9, 1989.

[11] W. Phillips, B. Towe, and P. Larson, "An ultrasonically-driven piezoelectric neural stimulator," in *Proc. 25th Annu. Int. Conf. IEEE Eng. Med. Biol.*, Sep. 2003, vol. 2, pp. 1983–1986.

[12] M. Southcott *et al.*, "A pacemaker powered by an implantable biofuel cell operating under conditions mimicking the human blood circulatory system-battery not included," *Phys. Chem. Chem. Phys.*, vol. 15, no. 17, pp. 6278–6283, May 2013.

[13] J. Gyu Bum and B. H. Cho, "An energy transmission system for an artificial heart using leakage inductance compensation of transcutaneous transformer," *IEEE Trans. Power Electron.*, vol. 13, no. 6, pp. 1013–1022, Nov. 1998.

[14] Q. Chen, S. C. Wong, C. K. Tse, and X. Ruan, "Analysis, design, and control of a transcutaneous power regulator for artificial hearts," *IEEE Trans. Biomed. Circuits Syst.*, vol. 3, no. 1, pp. 23–31, Feb. 2009.

[15] H. G. Lim, D. W. Kim, M. W. Lee, and J. W. Lee, "Intelligent pillow type wireless charger for fully implantable middle ear hearing system with a function of electromagnetic emission reduction," in *Proc. 2nd Int. Symp. Intell. Inf. Technol. Appl.*, 2008, pp. 835–838.

[16] Y. Zhou, X. J. Yu, J. M. Cheng, C. H. Wang, and L. Wang, "Transcutaneous energy transmission system for cardiac pacemaker," *Trans. China Electrotech. Soc.*, vol. 25, no. 3, pp. 48–53, Mar. 2010.

[17] A. Kurs, A. Karalis, R. Moffatt, J. D. Joannopoulos, P. Fisher, and M. Soljačić, "Wireless power transfer via strongly coupled magnetic resonances," *Science*, vol. 317, no. 5834, pp. 83–86, Jul. 2007.

[18] A. K. Ramrakhyani, S. Mirabbasi, and C. Mu, "Design and optimization of resonance-based efficient wireless power delivery systems for biomedical implants," *IEEE Trans. Biomed. Circuits Syst.*, vol. 5, no. 1, pp. 48–63, Feb. 2011.

[19] S. Raju, R. Wu, M. Chan, and C. P. Yue, "Modeling of mutual coupling between planar inductors in wireless power applications," *IEEE Trans. Power Electron.*, vol. 29, no. 1, pp. 481–490, Jan. 2014.

[20] C. Y. Xiao, Y. F. Liu, D. N. Cheng, and K. Z. Wei, "New insight of maximum transferred power by matching capacitance of a wireless power transfer system," *Energies*, vol. 10, no. 5, p. 688, May 2017.

[21] A. Trigui, S. Hached, F. Mounaim, A. C. Ammari, and M. Sawan, "Inductive power transfer system with self-calibrated primary resonant frequency," *IEEE Trans. Power Electron.*, vol. 30, no. 11, pp. 6078–6087, Nov. 2015.
[22] G. Monti, P. Arcuti, and L. Tarricone, "Resonant inductive link for remote powering of pacemakers," *IEEE Trans. Microw. Theory Techn.*, vol. 63, no. 11, pp. 3814–3822, Nov. 2015.
[23] T. Campi, S. Cruciani, F. Palandrani, and V. De Santis, "Wireless power transfer charging system for AIMDs and pacemakers," *IEEE Trans. Microw. Theory Techn.*, vol. 64, no. 2, pp. 633–642, Feb. 2016.
[24] C. Y. Xiao, K. Z. Wei, D. N. Cheng, and Y. F. Liu, "Wireless charging system considering eddy current in cardiac pacemaker shell: Theoretical modeling, experiments, and safety simulations," *IEEE Trans. Ind. Electron.*, vol. 64, no. 5, pp. 3978–3988, May 2017.
[25] H. Wieneke, T. Konorza, R. Erbel, and E. Kisker, "Leadless pacing of the heart using induction technology: A feasibility study," *Pacing Clin. Electrophysiol.*, vol. 32, no. 2, pp. 177–183, Feb. 2009.
[26] S. Kim, J. S. Ho, and A. S. Y. Poon, "Wireless power transfer to miniature implants: Transmitter optimization," *IEEE Trans. Antennas Propag.*, vol. 60, no. 10, pp. 4838–4845, Oct. 2012.
[27] J. I. Laughner *et al.*, "A fully implantable pacemaker for the mouse: From battery to wireless power," *Plos One*, vol. 8, no. 10, Oct. 2013, Art. no. e76291.
[28] C. Y. Xiao, K. Z. Wei, F. Liu, and Y. X. Ma, "Matching capacitance and transfer efficiency of four wireless power transfer systems via magnetic coupling resonance," *Int. J. Circuit Theory Appl.*, vol. 45, no. 6, pp. 811–831, Jun. 2017.
[29] H. H. Wu, A. Gilchrist, K. Sealy, and D. Bronson, "A 90 percent efficient 5 kW inductive charger for EVs," in *Proc. IEEE Energy Convers. Congr. Expo.*, 2012, pp. 275–282.
[30] U. K. Madawala and D. J. Thrimawithana, "A bidirectional inductive power interface for electric vehicles in V2G systems," *IEEE Trans. Ind. Electron.*, vol. 58, no. 10, pp. 4789–4796, Oct. 2011.
[31] S. Li, W. Li, J. Deng, T. D. Nguyen, and C. C. Mi, "A double-sided LCC compensation network and its tuning method for wireless power transfer," *IEEE Trans. Veh. Technol.*, vol. 64, no. 6, pp. 2261–2273, Jun. 2014.
[32] X. Qu, Y. Jing, H. Han, S. C. Wong, and C. K. Tse, "Higher order compensation for inductive-power-transfer converters with constant-voltage or constant-current output combating transformer parameter constraints," *IEEE Trans. Power Electron.*, vol. 32, no. 1, pp. 394–405, Jan. 2017.
[33] H. Feng, T. Cai, S. Duan, J. Zhao, X. Zhang, and C. Chen, "An LCC-compensated resonant converter optimized for robust reaction to large coupling variation in dynamic wireless power transfer," *IEEE Trans. Ind. Electron.*, vol. 63, no. 10, pp. 6591–6601, Oct. 2016.
[34] Vitatron G70 DR Dual Pacemaker System. [Online]. Available: http://www.vitatron.com/inserts/g70-dr.html
[35] H. Jiang *et al.*, "A low-frequency versatile wireless power transfer technology for biomedical implants," *IEEE Trans. Biomed. Circuits Syst.*, vol. 7, no. 4, pp. 526–535, Apr. 2013.
[36] E. P. Widmaier, H. Raff, and K. Strang, *Vander's Human Physiology: The Mechanisms of Body Function*. New York, NY, USA: McGraw-Hill, 2007, p. 626.
[37] A. Christ *et al.*, "Evaluation of wireless resonant power transfer systems with human electromagnetic exposure limits," *IEEE Trans. Electromagn. Compat.*, vol. 55, no. 2, pp. 265–274, Apr. 2013.
[38] International Commission on Non-Ionizing Radiation Protection, "Guidelines for limiting exposure to time-varying electric, magnetic, electromagnetic fields (up to 300 GHz)," *Health Phys.*, vol. 74, no. 4, pp. 494–522, Oct. 1998.
[39] IEEE Standard for Safety With Respect to Human Exposure to Radio Frequency Electromagnetic Fields, 3 kHz to 300 GHz, IEEE Standard C95.1, 2005.
[40] S. Gabriel, R. W. Lau, and C. Gabriel, "The dielectric properties of biological tissues: III. Parametric models for the dielectric spectrum of tissues," *Phys. Med. Biol.*, vol. 41, no. 11, pp. 2271–2293, Nov. 1996.

Chunyan Xiao (M'16) was born in Tongliao, China, in 1976. She received the B.S. degree in energy and power engineering and the Ph.D. degree in vehicle operation engineering from Beijing Jiaotong University, Beijing, China, in 1997 and 2002, respectively.

She was a Postgraduate Researcher in the Department of Electrical Engineering, Beihang University, Beijing, China. She is currently an Associate Professor of electrical engineering in the School of Automation Science and Electrical Engineering, Beihang University. Her research interests include wireless power transfer, electromagnetic nondestructive testing, and electromagnetic compatibility.

Dingning Cheng was born in Xianning, China, in 1994. She received the B.S. degree in electrical engineering and automation, in 2016, from Beihang University, Beijing, China, where she is currently working toward the M.S. degree in electrical engineering.

Her research interests include electromagnetic safety and thermal aspects of a wireless charging system equipped with a pacemaker.

Kangzheng Wei was born in Xi'an, China, in 1992. He received the B.S. degree in electrical engineering and automation, in 2014, from Beihang University, Beijing, China, where he is currently working toward the M.S. degree in electrical engineering.

His research interests include wireless charging system and its electromagnetic safety for cardiac pacemaker.